

Mechanistic Insights into Transition Metal-Catalysed Oxidation of a Hydroxamic Acid with *in situ* Diels–Alder Trapping of the Acyl Nitroso Derivative

Judith A. K. Howard,^a Gennadiy Ilyashenko,^a Hazel A. Sparkes,^a
Andrew Whiting,^{a,*} and Allen R. Wright^b

^a Department of Chemistry, Science Laboratories, Durham University, South Road, Durham DH1 3 LE, U.K.
Fax: (+44)-(0)191-386-1127; e-mail: andy.whiting@durham.ac.uk

^b School of Chemical Engineering and Advanced Materials, Merz Court, University of Newcastle, Newcastle upon Tyne NE1 7AR, U.K.

Received: December 4, 2007; Published online: March 25, 2008

Abstract: New insights into the mechanism for the transition metal-mediated oxidation of hydroxamic acids to give intermediate acyl nitroso species, with subsequent hetero-Diels–Alder trapping are presented. The activation of triphenylphosphine-ligated ruthenium-salen complexes is examined, and evidence is presented for the ruthenium-oxo species which are involved in the oxidative process of the hydroxamic acid. The observation of the lack of asymmetric induction involved in the intermolecular cycloaddition process involving the intermediate acyl

nitroso species is explained, with the aid of comparing the ruthenium-salen-based systems with nitrosotoluene, and copper(I)/copper(II) BINAP-based catalysis of nitrosopyridine complexes. This study demonstrates the importance of secondary coordination to achieve asymmetric induction in nitroso-Diels–Alder reactions.

Keywords: hetero-Diels–Alder reaction; oxidation; oxo ligands; ruthenium

Introduction

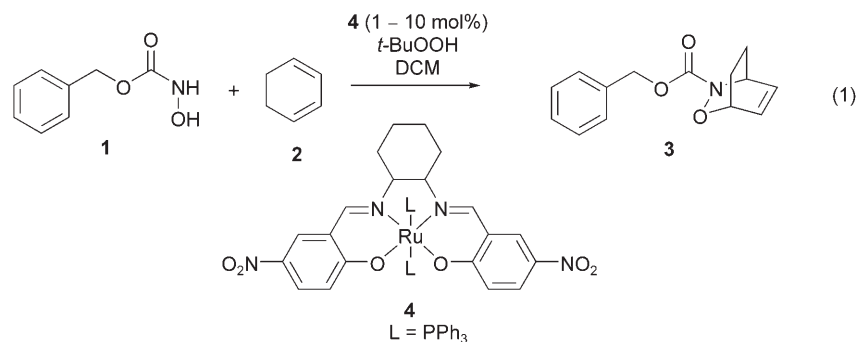
The use of nitroso compounds as efficient hetero dienophiles in [4+2] cycloaddition reactions with conjugated dienes to produce 3,6-dihydro-1,2-oxazines has been studied for over half a century.^[1] These types of hetero-Diels–Alder (DA) reactions have been used as powerful synthetic tools in the formation of natural products such as polyhydroxylated alkaloids and their derivatives.^[2,3] In addition to well established stoichiometric oxidative processes,^[4] there are a few transition metal-based catalysts which are capable of oxidising hydroxamic acids to their corresponding nitroso species.^[5,6] Despite numerous attempts to carry out an asymmetric version of this transformation only limited success (low *ee*) was achieved for intermolecular cycloaddition,^[7] however, much improved asymmetric induction has been achieved in intramolecular nitroso-Diels–Alder reactions.^[8] The low *ees* in intermolecular cases and good levels of asymmetric induction in intramolecular cases poses a question about the involvement of the catalyst in these DA reactions. If the dissociation of an oxidised species from the catalyst, or re-oxidation of the catalyst is faster than the subsequent DA reaction, then the product would be race-

mic. The opposite is also true: if the dissociation of the oxidised species or re-oxidation is slower than the DA reaction, then the product should show some level of enantiomeric induction. It is possible that intramolecular DA reactions form products with good levels of asymmetric induction, while the corresponding intermolecular reactions do not, because their reactions are much faster. Although, this hypothesis has been postulated previously^[8] no robust mechanistic studies had been carried out. Our long-term interest is to develop systems for the oxidation of hydroxamic acids with asymmetric *in situ* DA trapping of the acyl nitroso derivative,^[5,7] to this end detailed mechanistic studies of the reactions have been carried out and herein we report our results.

Results and Discussion

Mechanism Studies on *in situ* Generated Acyl Nitroso Compounds

In order to detect possible intermediates in the ruthenium-salen-mediated oxidation of a hydroxamic acid a combination of techniques was employed; time-re-



solved infrared spectroscopy using ReactIR, mass spectrometry and concentration profiles being obtained from $^1\text{H NMR}$ spectroscopy. The results of these experiments were utilised to construct a reaction network in order to postulate possible reaction mechanism(s). The initial model reaction studied was the Ru(salen) **4** catalysed oxidation of *Z*-protected hydroxamic acid **1** [Eq. (1)] with *t*-BuOOH and the subsequent trapping of acyl nitroso species with a diene **2**. The imine shifts of the ruthenium complex were monitored by IR which it was thought would provide a direct probe for the coordination environment of ruthenium during the reaction as well as providing structural information on any important catalytically active species. Mass spectrometry was also employed to try and confirm the identity of short-lived intermediates, while time-resolved $^1\text{H NMR}$ spectroscopy was used to measure quantitatively the concentrations of **1**, **2** and **3** during the reaction and enable kinetic analysis.

Initially, the reaction shown in Eq. (1) was studied using time-resolved IR spectroscopy. Stoichiometric reactions between each component of the reaction mixture (**1**, **2** and oxidant) and the catalyst **4**, were set up to investigate the interactions between each of the reactant species and the catalyst. No changes were observed in the IR spectrum when either hydroxamic acid **1** or the diene **2** were mixed with **4**, in both cases this indicates that there are no interactions between either **1** or **2** and **4**. However, upon addition of the oxidant to **4**, a new absorption peak corresponding to the formation of $\text{O}=\text{PPh}_3$ appeared at $1250\text{--}1300\text{ cm}^{-1}$ (see Figure 1, top). More interestingly was the simultaneous appearance of a weak absorption peak around 830 cm^{-1} (see Figure 1, bottom), which can be assigned to an $\text{Ru}=\text{O}$ stretch.^[9] The existence of species **5a** and **5b** in the reaction mixture was confirmed by mass spectrometry with the appearance of ions at $m/z = 529$ for **5a** and 791 for **5b**. Based upon these observations and by drawing analogies with the chromium(V)oxo(salen) species reported by Kochi,^[10] we propose that the active catalyst is Ru(oxo)(salen) **5a**. It is most likely that **5a** is formed by the dissociation of PPh_3 from complex **5b** which had arisen from

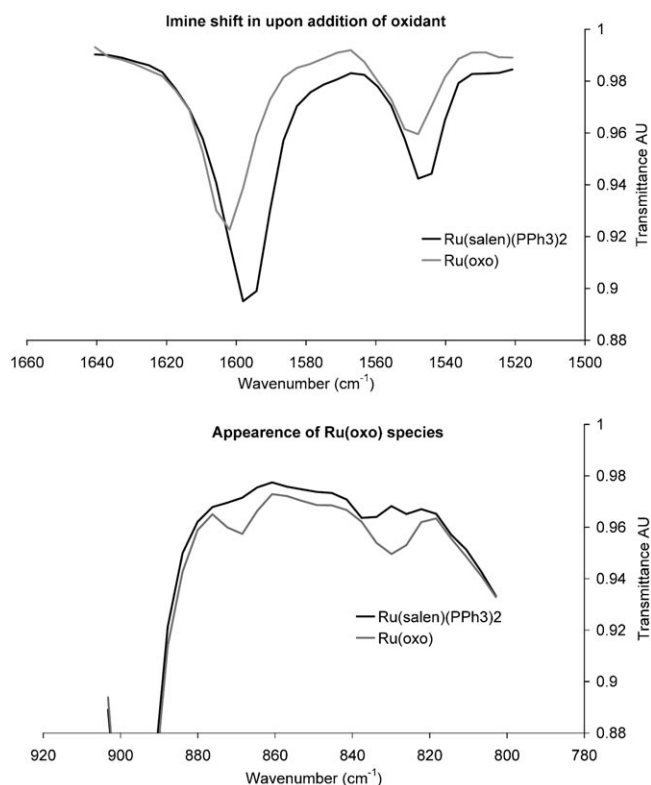
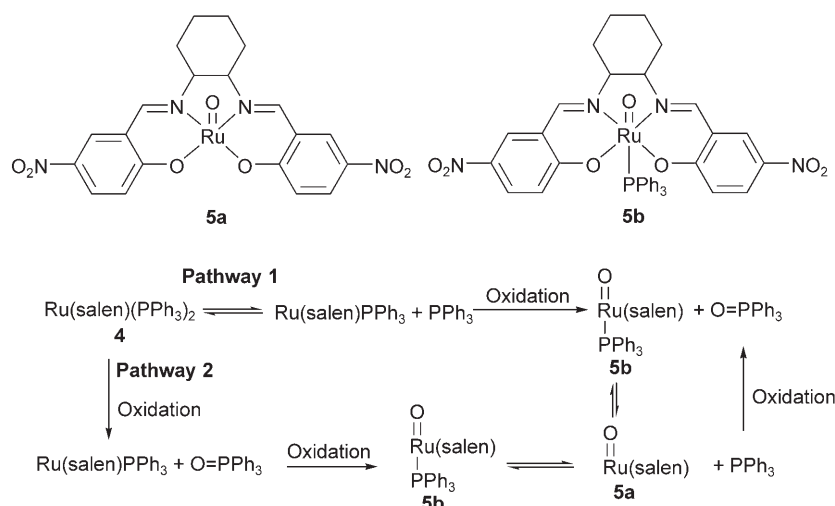


Figure 1. Structure of proposed active catalyst **5a** or **5b** and ReactIR snapshots were generated using Excel: *top*, expanded imine region; *bottom*, expanded $\text{Ru}=\text{O}$ region.

the initial oxidation of the Ru(salen) complex **4**. The oxidation of **4** to give **5b** can occur *via* two possible routes, as shown in Scheme 1. In *pathway 1*, an equilibrium is established between **4** and a species in which PPh_3 has dissociated from the metal centre. Upon the addition of oxidant both PPh_3 and Ru(salen) PPh_3 are oxidised to triphenylphosphine oxide and **5b**, respectively, hence, the equilibrium shifts to the right until none of complex **4** remains. The alternative, *pathway 2*, would involve nucleophilic attack of the oxidant on PPh_3 while it is still attached to the metal centre, resulting in oxidation of PPh_3 and dissociation from the metal centre. Which-



Scheme 1. Two possible pathways towards the oxidation of $\text{Ru(salen)(PPh}_3)_2$ to Ru-oxo complex **5a**.

ever pathway is followed, complex **5b** forms initially and is then converted to the active catalyst **5a**.

The ReactIR studies carried out on the reaction outlined in Eq. (1), also indicated that catalase-like (dioxygen evolution) activity of the ruthenium complex **4** (or its derivative **5a** and **5b**) was negligible. In fact, it is only when hydroxamic acid **1** is added to the reaction mixture containing all of the components, including oxidant that the reaction is initiated. Time-resolved IR monitoring of the oxidation process clearly showed the formation of water in the reaction mixture (see Figure 2), the absorption peak at approximately 1700 cm^{-1} was assigned to hydroxamic acid **1** while the broad peak around 1650 cm^{-1} corresponds to the formation of water during the oxidation process. Despite extensive efforts to quantify the data,

these results remain qualitative due to the complexity of the spectra and changes in the base line over time. It was also not possible to monitor the formation of the acyl nitroso species using ReactIR as the absorptions corresponding to compounds **1** and **3** overlap and were further masked by the water absorption. However, it is possible to draw the following conclusions: firstly, there were no detectable interactions between **1** or **2** and **4** which might have indicated an intermediate species; secondly, the catalase activity of complex **4** is negligible; thirdly, the oxidation of hydroxamic acid **1** is fast and is most likely to result from oxidation by an Ru=O complex, either **5a** or **5b**, formed *in situ* in the manner described above.

The ^1H NMR spectroscopic studies were carried out on each of the reactions described in Eq. (1) and Eq. (2),

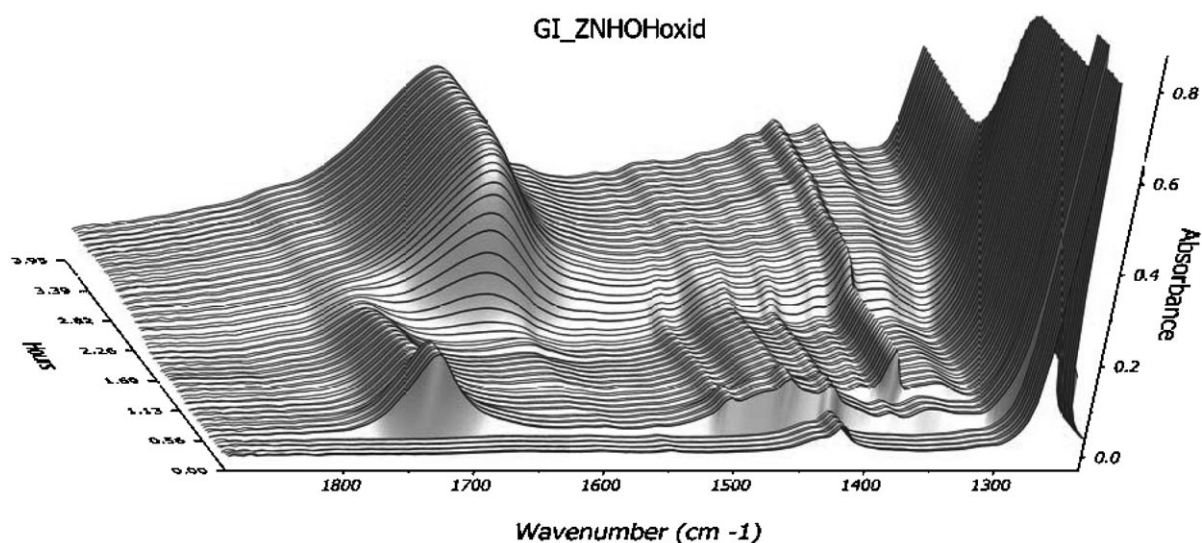
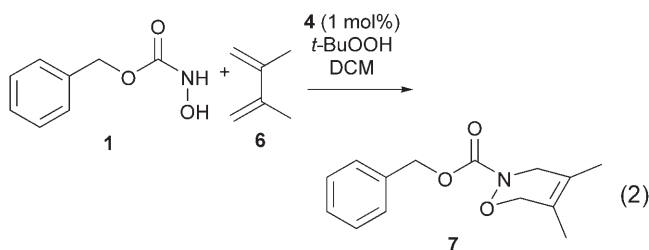


Figure 2. Relevant part of the ReactIR spectrum obtained during catalytic reaction described in Eq. (1).



using anisole (100 mol%) as internal standard. Reactions were followed over time to determine the rate of conversion of starting materials to products and the results are shown in Figure 3.

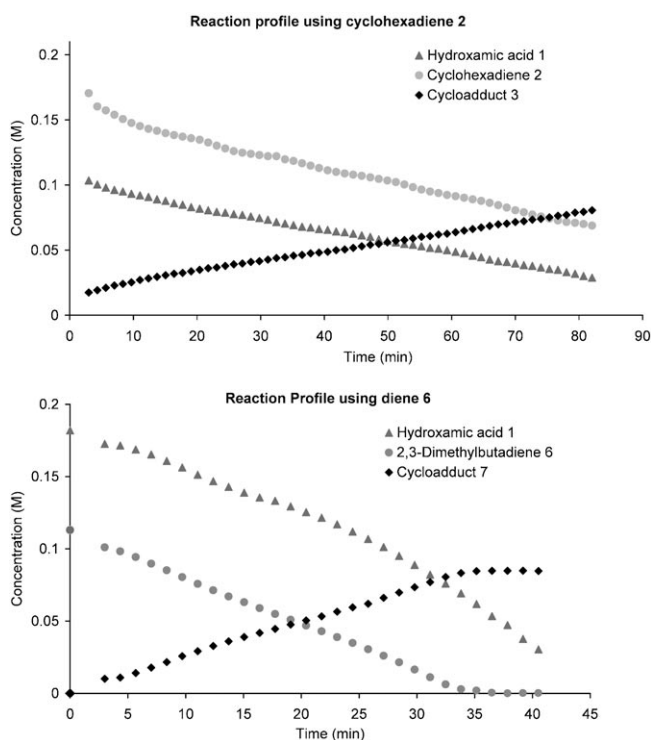
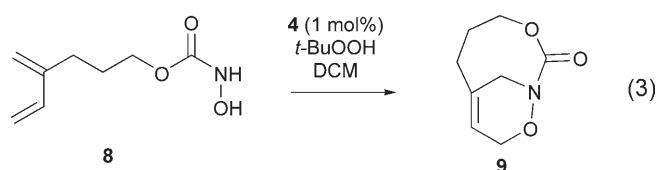


Figure 3. ^1H NMR-spectroscopy derived concentration profiles for the reactions described in Eqs. (1) and (2) using: *top*, cyclohexadiene **2**; *bottom*, 2,3-dimethylbutadiene **6**.

The concentration profiles obtained from the ^1H NMR spectroscopy measurements (Figure 3) suggest that the rate of each of the reactions described by Eq. (1) and Eq. (2) is controlled by the catalytic oxidation of **1** by **4**, that is, the simultaneous disappearance of both starting materials and concomitant appearance of the product occur at the same rate (within experimental error). This indicates that as soon as the nitroso intermediate is produced through the oxidation, it is essentially consumed instantly by the diene. If the diene is used as the limiting reagent, then it is consumed completely to form the cycloadduct in quantitative yield, if oxidation of the hydroxa-

mic acid had continued, it would have resulted in side products arising from decomposition of the nitroso intermediate; these were not identified. Attempts were made to monitor these reactions using an increased catalyst loading of 5 mol%, however, this resulted in the reactions occurring at such a fast rate that it was impossible to obtain meaningful NMR spectroscopic data. In accordance with previous findings, the use of enantiomerically pure catalyst **4** in these intermolecular reactions resulted in the formation of racemic products.^[5]

In conjunction with the intermolecular study, the intramolecular reaction [Eq. (3)] of Shea et al.^[8] was



also investigated using the same approach. This reaction has been shown to proceed with good levels of asymmetric induction when an enantiomerically pure catalyst **4** is employed.^[8] As with the intermolecular reactions, the concentration of starting materials and products could be followed over time using ^1H NMR spectroscopy (Figure 4).

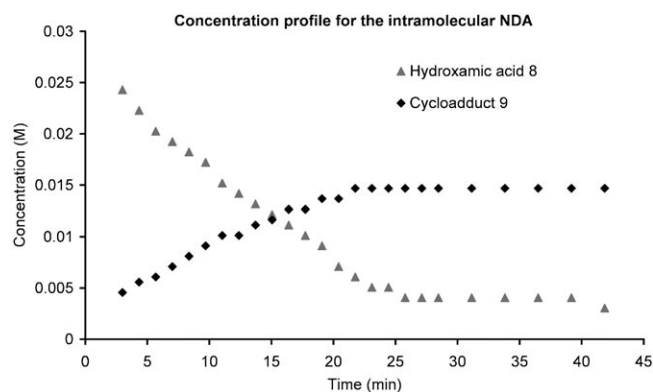


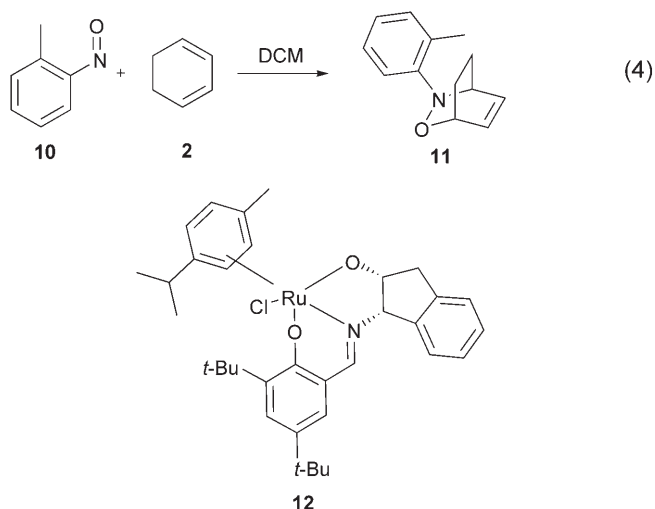
Figure 4. ^1H NMR spectroscopy-derived concentration profile for the intramolecular reaction described in Eq. (3) using hydroxamic acid **8**.

Unsurprisingly, Figure 4 shows a similar linear profile to those shown in Figure 3, however, the non-quantitative conversion of starting material to product was not expected, i.e., there is a clear mass imbalance shown in Figure 4. After approximately 24 min, most of the starting hydroxamic acid had been consumed, but only approximately 2/3 of the expected product had been produced. It has been postulated that the observed enantiomeric excess can be explained by the

assertion that the intramolecular Diels–Alder reaction is faster than dissociation of the nitroso species from the ruthenium catalyst.^[8] Indeed, if Diels–Alder cyclisation is faster than the dissociation process, the starting material would be expected to be converted quantitatively into product. Since this is not the case, as demonstrated graphically by Figure 4, the implication is that the acyl nitroso species does dissociate from the ruthenium-salen catalyst species faster than intramolecular cyclisation can occur, and although cyclisation does occur, it is in competition with decomposition of the intermediate nitroso species. In addition, when product **9** [Eq. (3)] was isolated it was found to be racemic. Further experiments were undertaken in an attempt to prepare the cycloadduct **9** in an enantiomerically enriched form, including carrying out the reaction at lower temperatures, however, these failed to produce any sign of asymmetric induction.

Mechanism Studies on *ortho*-Nitrosotoluene

The results obtained thus far all seemed to indicate that the oxidation of each of the hydroxamic acids employed in Eqs. (1)–(3) is the controlling step in each of the reactions and, therefore, it necessary to investigate the kinetics of nitroso-Diels–Alder cycloaddition independently of the oxidation process. Unfortunately, the instability of the intermediate acyl nitroso species involved in Eqs. (1)–(3) means that these types of reactive species could not be used for the desired kinetic experiments and so attention was turned to more stable nitroso derivatives, starting with *ortho*-nitrosotoluene **10**. In the first instance, kinetic investigations into the thermal nitroso-cycloaddition reaction were undertaken between **10** and cyclohexadiene **2** [Eq. (4)]. This reaction was followed over time by ¹H NMR as described above, and modelling of the reactant/product profile was carried out



using BatchCADTM^[11] to provide the results shown in Figure 5.

From the data presented in Figure 5, it can be seen that the reaction shown in Eq. (4) follows simple

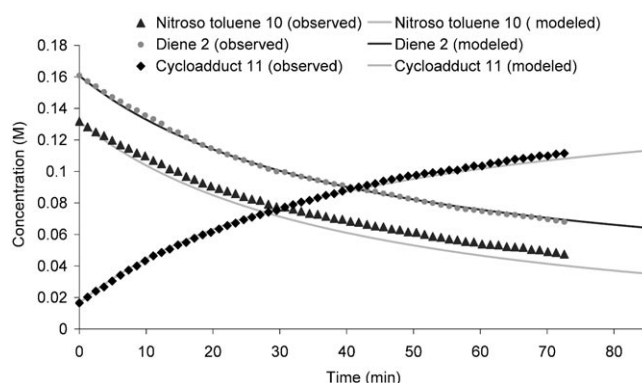


Figure 5. Concentration profile for the thermal reaction described in Eq. (4), experimental (as determined by ¹H NMR spectroscopy) and calculated (modelled using BatchCADTM).

second-order kinetics, with $k = 2.2 \times 10^{-3} \text{ s}^{-1} \text{ M}^{-1}$ {rate = $k \cdot [\text{cyclohexadiene}] [\text{nitrosotoluene}]$ } (obtained by UV/vis spectroscopy). The concentration profiles obtained experimentally by ¹H NMR methods were similar to those obtained using BatchCADTM ¹¹ (Figure 5). In addition, the calculated rate constant ($k = 2.7 \times 10^{-3} \text{ s}^{-1} \text{ M}^{-1}$) showed good agreement with that obtained experimentally by UV/vis spectroscopy. In order to compare the kinetics of the thermal cycloaddition reactions with the corresponding catalysed reactions, the effect of including catalysts **4** and **12** into the reaction [Eq. (4)] was investigated. The results of these experiments are summarised in the reaction profiles shown in Figure 6.

The results shown in Figure 6 clearly show that catalyst **12** has no effect, whereas catalyst **4** actually reduces the rate of product formation to a small degree. Closer examination of reaction profile revealed that, in all cases, nitrosotoluene **10** was consumed at approximately the same rate, whereas cyclohexadiene **2** was consumed slightly slower in the presence of Ru(salen) **4**. It can, therefore, be postulated that the negative effect in the rate of cycloaddition can be attributed to the competing side reaction of the oxidation of triphenylphosphine by nitrosotoluene after it has been released from the catalyst. In fact, the reaction of free triphenylphosphine (1 equiv.) with nitrosotoluene (1 equiv.) at room temperature is rapid (complete in *ca.* 5 min) and indeed produces triphenylphosphine oxide and 2-methylaniline in almost quantitative yields.

We have previously shown that complexes **12**, **13** and **15** were active catalysts in the oxidation of hy-

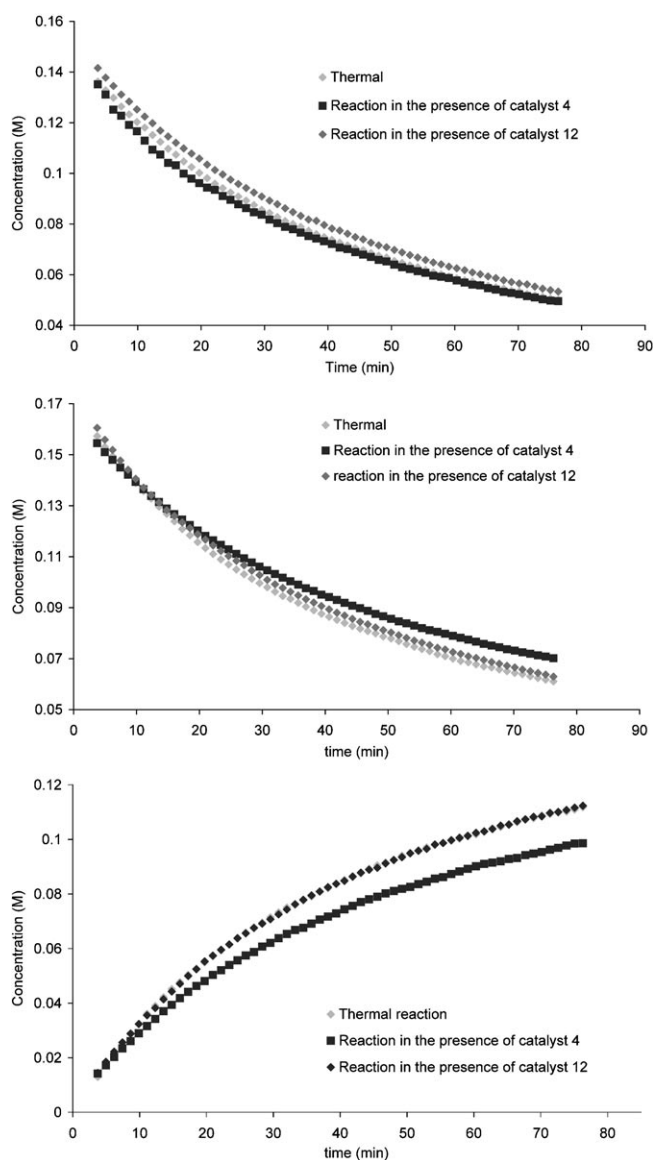


Figure 6. ^1H NMR derived study showing the effect of the catalysts **4** (10 mol%) and **12** (2 mol%) on the nitroso-Diels–Alder reaction shown in Eq. (4). *top*: consumption of nitrosotoluene **10**; *middle*: consumption of diene **2**; *bottom*: formation of cycloadduct **11**.

droxamic acid to nitroso species, albeit the subsequent nitroso-Diels–Alder reaction proceeded with no asymmetric induction.^[5c] Since then we have expanded our study to include complexes **14**^[12] and **16**. Prompted by Yamamoto's report that Cu(I)-BINAP complexes produced high *ee* in nitroso-Diels–Alder reactions^[13] we have also decided to include in this study complexes **18** and **19** with analogous Ru(BINAP) **20**^[14] and another ruthenium complex **17** containing a ligand with chiral phosphorus.^[15] All of these complexes **12–20** were screened in the reaction and compared to the catalysts **4** at room temperature and at -78°C . In all cases the yields were similar to

those obtained for thermal reaction and no asymmetric induction was observed which confirms that nitroso species are poor coordinating ligands.

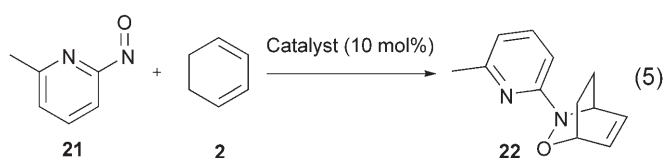
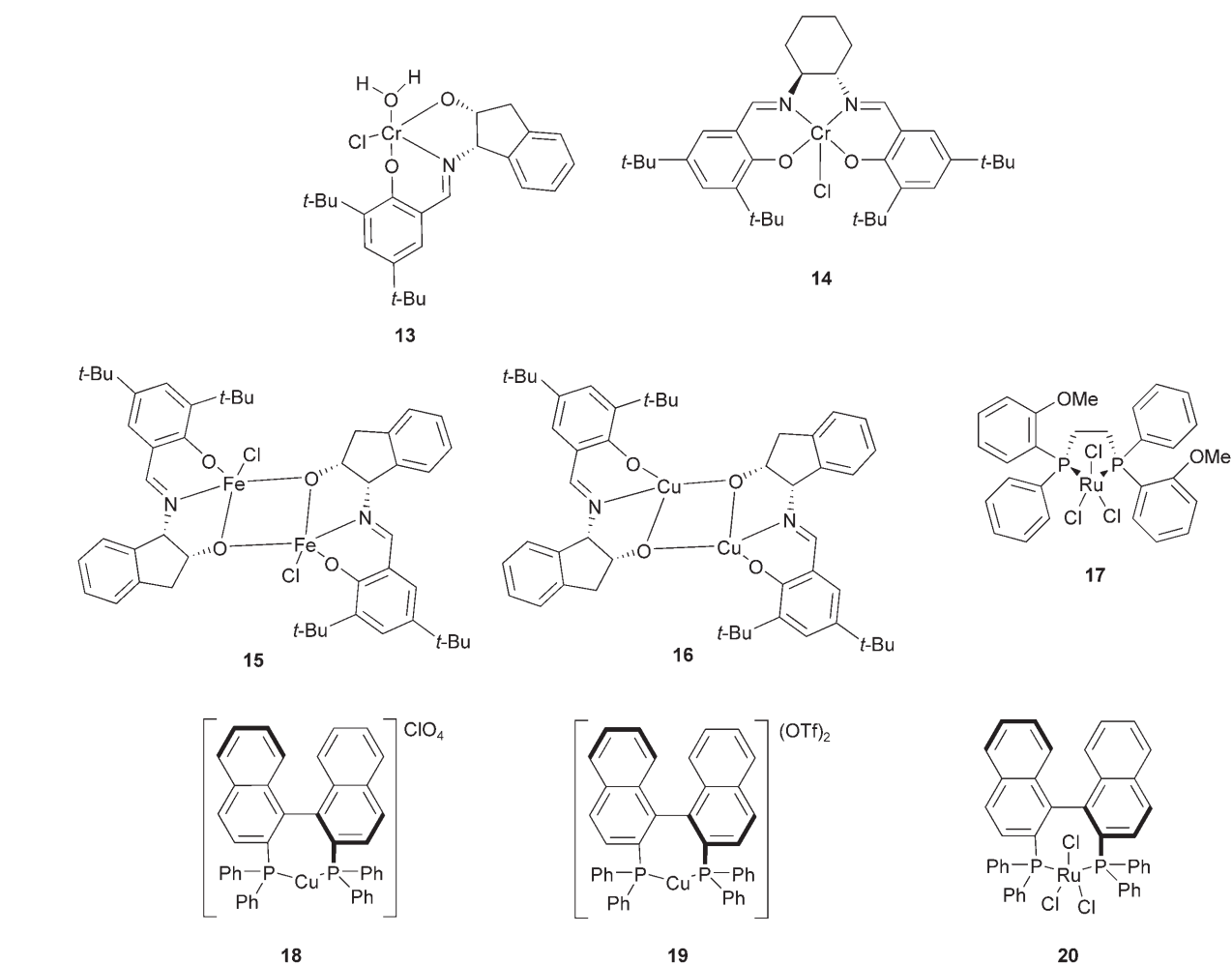
Mechanism Studies on 6-Methyl-2-nitrosopyridine

As illustrated above, the nitroso group is a poor coordinating ligand for ruthenium, which means that the most likely explanation for the lack of the catalytic activity of the ruthenium-based catalysts towards the nitroso-Diels–Alder reactions is the absence of a suitable binding function to enable the catalyst and substrate to interact. In order to overcome this problem, one needs to have an extra binding motif on the substrate to provide further coordination to the metal centre. Indeed, Yamamoto has elegantly illustrated this by use of 6-methyl-2-nitrosopyridine **21** which reacts with diene **2** in the presence of Cu(I)-BINAP complex to give an enantiomerically enriched cycloadduct **22** [Eq. (5)].^[13]

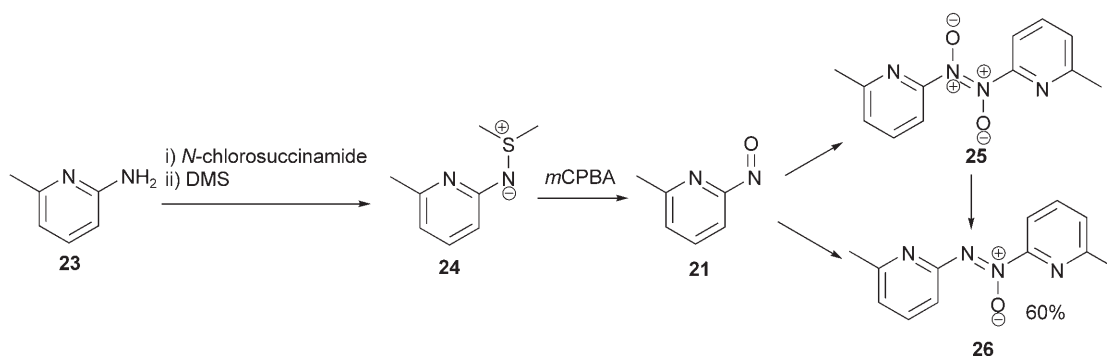
Following previously described protocols,^[13,16] the synthesis of nitrosopyridine **21** was attempted in order to compare the kinetics of its reaction with those discussed above. The synthesis of nitrosopyridine **21** involves the *m*CPBA-mediated oxidation of the corresponding ylide **24**, which was formed from aminopyridine **23** as outlined in Scheme 2, however, instead of isolating the expected nitroso compound **21**, the azo mono-oxide **26** was isolated as the major component, the structure of which was confirmed by single crystal X-ray crystallography (Figure 7). Further investigation showed that the presence of unreacted starting material **23** triggers the disproportionation of dimeric azo di-oxy species **25** to give **26**. The separation of **24** and **23** is not possible at an earlier stage of the reaction, and the oxidation of **24** occurs with predominant formation of the by-product **26**. This can be largely circumvented by carrying out the oxidation of **24** at lower temperature, and once the solvent is removed after the oxidation step, the resulting mixture can be loaded on to a column and purified allowing separation of **21** and **23**. Although the decomposition of **21** or **25** to **26** still occurs, it is at much reduced rate and both compounds can be obtained as reasonably stable solids. It is worth noting that **26** can seemingly not be re-oxidised to **25** or **21** under the reaction conditions and is completely inert in the nitroso-Diels–Alder reaction.

Since the synthesis of **21** could be capricious and low yielding, we attempted to eliminate the isolation of **21** and instead carry out the oxidation of **24** to **21** directly, with subsequent nitroso-Diels–Alder trapping *in situ* using complexes **4** and **12–16** as potential catalysts [Eq. (6)].

Of the various combinations of the catalysts and oxidants examined [Table 1, Eq. (6)], most proved to



be largely unsuccessful, with the notable exception of the iron-based catalyst **15** (entries 5 and 7) which when used in conjunction with H_2O_2 at room temperature or peracetic acid at -78°C in acetone gave the nitroso cycloadduct **22** in 42% and 47% yields, respectively (both racemic). To the best of our knowledge, this is the first example of the *in situ* generation of the nitroso species **21**, and considering the intricacy



Scheme 2. Decomposition of nitrosopyridine **21** to **26**.

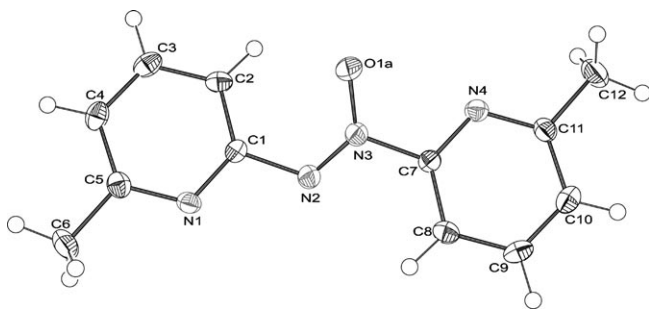
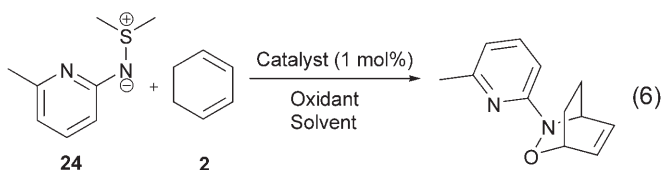


Figure 7. X-ray crystal structure of azo-oxide **26**, ellipsoids are depicted at the 50% probability level. Hydrogen atoms are shown as spheres of arbitrary radius. For clarity only one position is shown for O1 (labelled O1a).



cies of the formation of **21** as a pure reagent and its lack of commercial availability, this may be a useful finding applicable in other reactions, such as the nitroso-aldol and related reactions.^[17]

The thermal cycloaddition between nitrosopyridine **21** and diene **2** under the conditions identical to those used for nitrosotoluene proceeded much faster (*ca.* < 5 min *versus* 100 min, respectively) and it was therefore not possible to employ ¹H NMR spectroscopy to obtain a starting material/product reaction profile. The nitrosopyridine **21** exists in organic solvents in an equilibrium between the azo-monomer and di-oxide dimer, since their UV chromophores overlap, the use

of UV/Vis spectroscopy to follow the reaction was also not possible. Therefore, it was decided to screen available catalysts shown above in this reaction, under the conditions described by Yamamoto,^[13] in order to use asymmetric induction to probe the cycloaddition [Eq. (5)] further, the results are presented in Table 2.

A combination of Cu(I) with (*R*)-BINAP (entry 3) yielded product **22** in an 88% yield with a 65% *ee* which although lower than the *ees* reported by Yamamoto,^[13] was essentially as expected. In contrast, employing complexes **4**, **12–15**, **17** and **20** (entries 4–8, 10 and 12) gave identical results to the thermal reaction (entry 2) with 100% conversion and 0% *ee*. On the other hand, when Cu(II) complex **16** was used (entry 9), **22** was produced with an 84% yield and 13% *ee*. This indicates that Cu(II) complexes may be used as catalysts in these types of cycloaddition reactions, and it raises the question of whether they may in fact be preferable to Cu(I) complexes, which might be sensitive to the potentially oxidising conditions created by the presence of nitrosopyridine **21**. In order to probe this mechanistic point further, the use of Cu(I) in the original protocol^[12] was replaced by Cu(II) in the same reaction (entry 12). When the reaction was complete, **22** was isolated in an 89% yield with a 50% *ee*. Further investigation into the Cu(II)-(*R*)-BINAP-catalysed reaction of **2** with nitrosopyridine **21** at -85°C was carried out, monitoring the *ee* of product **22** over time (entry 13). Aliquots were collected every hour for 7 h and analysed using HPLC, however, the enantiomeric excess remained constant at approximately 10% throughout the reaction. Upon increasing of the temperature to -20°C the *ee* improved dramatically to 45% and further investigations revealed that at or below -70°C both the catalysed

Table 1. Screening of various conditions for the reaction described in the Eq. (6).

Entry	Catalyst [1 mol%]	Oxidant	Solvent	Temperature [$^{\circ}\text{C}$]	Time [h]	Yield ^[a] [%]	<i>ee</i> [%]
1	-	H ₂ O ₂	Acetone	22	16	0	-
2	-	CH ₃ CO ₃ H ^[b]	MeCN	22	2	38	0
3	-	<i>m</i> CPBA	DCM	22	2	33	0
4 ^c	FeCl ₃	H ₂ O ₂	Acetone	22	1	0	-
5	15	H ₂ O ₂	Acetone	22	16	42	0
6 ^[c]	15	CH ₃ CO ₃ H ^[b]	MeCN	22	2	15	0
7	15	CH ₃ CO ₃ H ^[b]	Acetone	-78	8	47	0
8	15	<i>m</i> CPBA	DCM	-40	8	0	-
9	4	<i>t</i> -BuOOH	DCM	22	16	0	-
10	4	<i>m</i> CPBA	DCM	-40	16	0	-
11	12	H ₂ O ₂	Acetone	22	16	0	-
12	13	H ₂ O ₂	Acetone	22	16	0	-
13	14	<i>m</i> CPBA	DCM	-40	8	0	-
14	16	CH ₃ CO ₃ H ^[b]	MeCN	22	16	10	0

^[a] Isolated yields.

^[b] Peracetic acid was prepared by stirring acetic acid and H₂O₂ over Amberlite 400 resin to give 25% w/v solution.

^[c] Disproportionation of oxidant was observed.

Table 2. Screening of catalysts in asymmetric nitroso-Diels–Alder reaction as shown in Eq. (5).

Entry	Catalyst [10 mol%]	Temperature [°C]	Conversion [%] ^[a]	Yield [%] ^[b]	ee [%] ^[c]
1	-	25	100	88	0
2	-	–85 to –20 ^[d]	100	91	0
3	18	–85 to –20 ^[d]	100	88	65
4	4	–85 to –20 ^[d]	100	-	0
5	12	–85 to –20 ^[d]	100	-	0
6	13	–85 to –20 ^[d]	100	-	0
7	14	–85 to –20 ^[d]	100	-	0
8	15	–85 to –20 ^[d]	100	-	0
9	16	–85 to –20 ^[d]	100	84	13
10	17	–85 to –20 ^[d]	100	-	0
11	20	–85 to –20 ^[d]	100	-	0
12	19	–85 to –20 ^[d]	100	89	50
13	19	–85	<10	-	10
14	19	–70 to –55 ^[e]	100	90	60

^[a] Defined as% of starting material consumed.

^[b] Only isolated yields are quoted unless otherwise stated.

^[c] Obtained from HPLC.

^[d] Reaction initiated at –85°C, held at that temperature for 1 hour and then allowed to warm up to –20°C over 5 h period at which point it was held there for additional hour before allowing to reach room temperature.

^[e] The temperature was maintained in this window using cryostat.

and thermal reactions were negligible, whereas above –55°C, the thermal reaction contributed significantly to the product formation. When the reaction temperature was maintained between –70 and –55°C and allowed to proceed for 24 h, the final product **22** was obtained in 90% yield and 60% *ee* (Entry 14), i.e., essentially matching the results reported above for the Cu(I)-based system.

In order to gain further insight into the reaction mechanisms involved in the Cu(I) *versus* Cu(II)-catalysed cycloaddition reactions [Eq. (5)], it was decided to study the electrochemistry of nitrosopyridine **21**, together with the Cu(I)- and Cu(II)-(BINAP) complexes, and compound **26**. These experiments were carried out in dichloromethane (DCM) using all Pt electrodes, with Bu₄NPF₆ as the electrolyte and ferrocene as an internal reference. The results of these experiments are shown in Figure 8.

The cyclic voltammogram of the free BINAP ligand showed two irreversible oxidation processes at 1.19 V and 1.54 V (Figure 8, top). Upon coordination with copper, these oxidation events shifted to 1.25 V and 1.61 V, respectively, likely a consequence of the increased coulombic charge on the complex; under the conditions employed, the Cu(I)/Cu(II) couple was not observed. Cyclic voltammetry of nitrosopyridine **21** showed two reversible waves with different peak currents, the first $\Delta E_p = -0.69$ V and the second $\Delta E_p = -1.16$ V (Figure 8, middle). Initially, it was believed that these two potentials were due to monomer-dimer equilibration, however, it was later confirmed that the second wave ($\Delta E_p = -1.16$ V) was due to the disproportionation product **26**.

The voltammogram, therefore, has the characteristics of an ECE process. Finally, a series of tests to check for interactions between nitrosopyridine and Cu(I) were carried out (Figure 8, bottom). As expected, no interactions were observed between the Cu(I) salt and nitrosopyridine **21** in DCM, which is most likely to be due to the poor solubility of the metal salts in this solvent. Upon the addition of BINAP to this suspension, the concentration of nitrosopyridine **21** dramatically decreased, while the concentration of the disproportionation product **26** appeared to increase. Nitroso species are known to be good oxidants^[14] and, under the experimental conditions, nitrosopyridine **21** appears to be similar to molecular oxygen in its ability to carry out oxidations, which implies that Cu(I) is oxidised to Cu(II) under these reaction conditions. Furthermore, the natural tendency of nitrosopyridine **21** to disproportionate can be further enhanced by the presence of Cu(I). Thus, these results seem to demonstrate that the Cu(I)-(BINAP) complex is oxidised to Cu(II)-(BINAP) in the presence of nitrosopyridine **21**, and that it is actually the Cu(II)-(BINAP) complex that catalyses the reaction described in Eq. (5).

Proposed Mechanism

When all of the above is taken into consideration, a network of reactions can be proposed for the Ru(salen)(PPh₃)₂ **4** catalysed oxidation of a hydroxamic acid such as **1**, with *in situ* Diels–Alder trapping

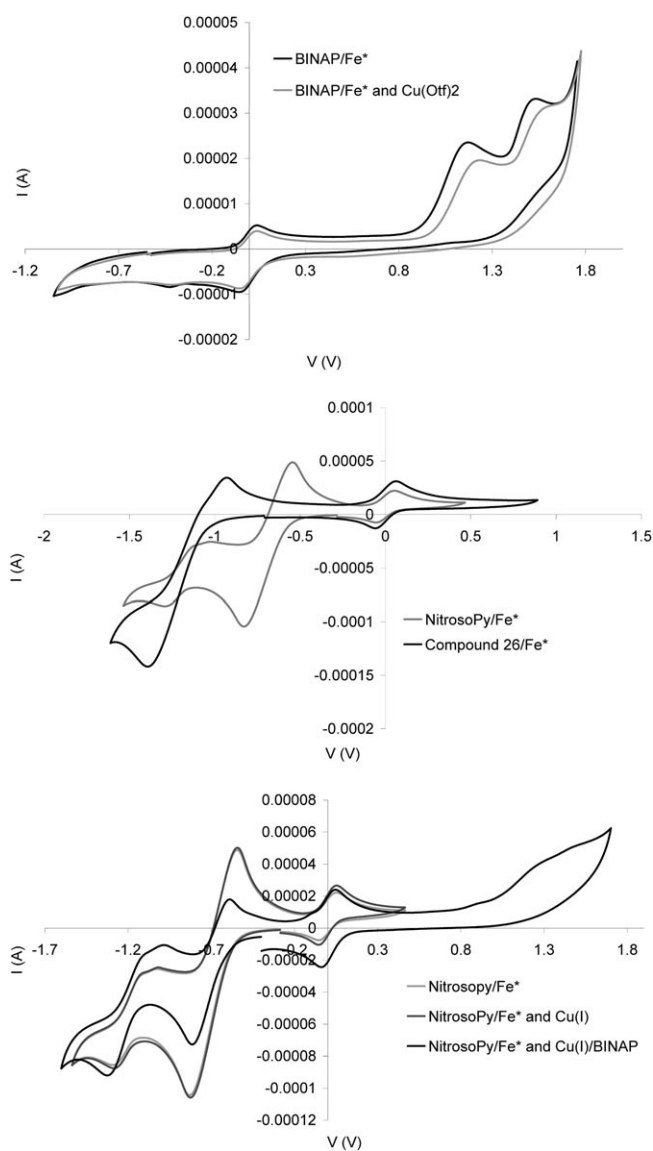


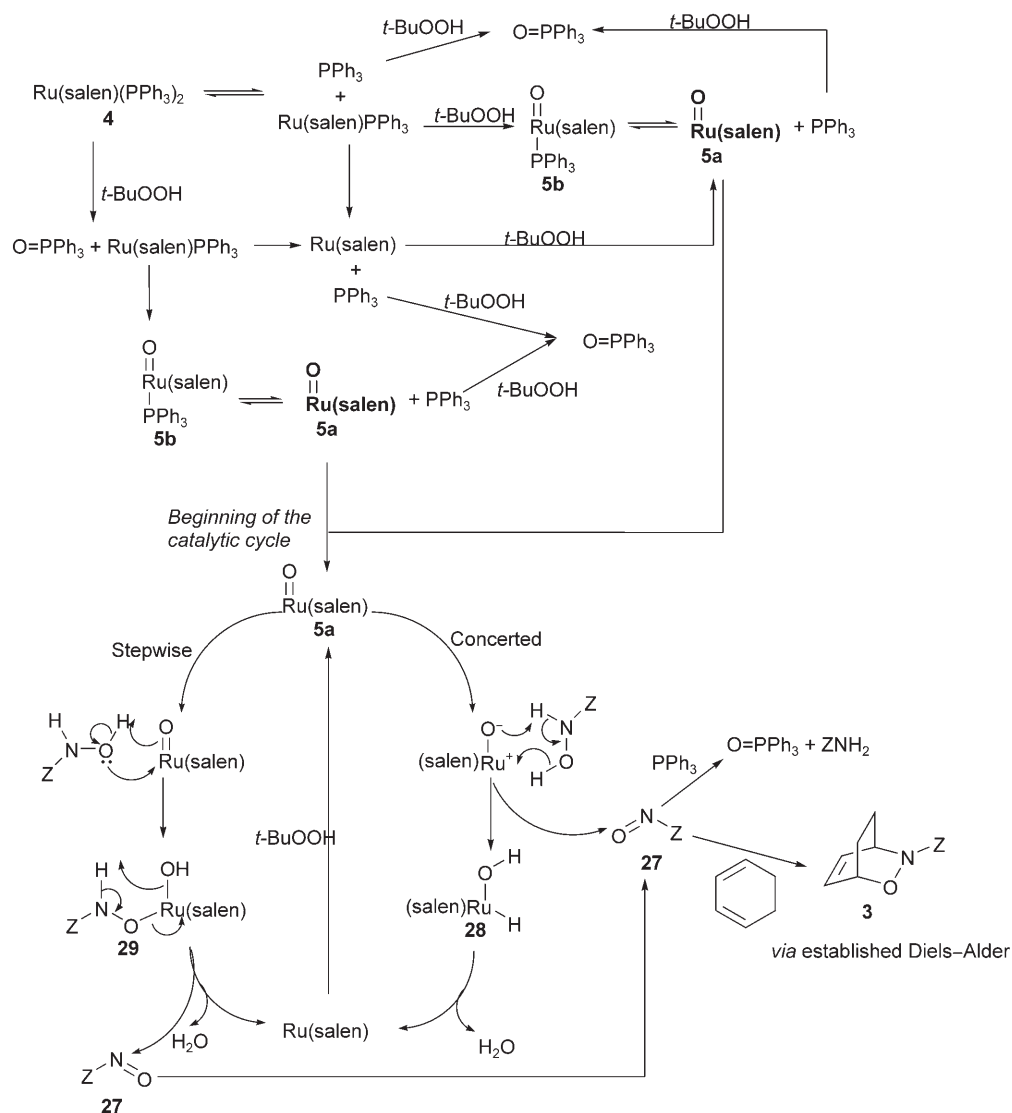
Figure 8. Cyclic voltammetry measurements for: *top*: reversible reduction of BINAP; *middle*: reduction of nitrosopyridine **21** and compound **26**; *bottom*: change in CV upon addition of Cu(I)(OTf) and BINAP.

of the acyl nitroso derivative (Scheme 3). The overall reaction can be broken down into three parts: oxidation of the metal catalyst into the active oxo-species, which subsequently oxidises hydroxamic acid to the nitroso species, and finally, a hetero-Diels–Alder cyclisation to give the product.

Although the oxidation of catalyst **4** into the active Ru(salen)(oxo) species has already been discussed (Scheme 1), further comments are warranted. Ru(salen)(PPh₃)₂ **4** is an electron-rich 18e⁻ complex, hence it is unlikely that conversion to the Ru(oxo) species would occur *via* nucleophilic attack of the oxidant on either the phosphine ligand or the metal

itself. It is therefore postulated that dissociation of the phosphine ligand must occur first to give Ru(salen)PPh₃ and free phosphine, both of which are then oxidised to the corresponding oxo-species **5a** or **5b**, and triphenylphosphine oxide side product, respectively. Since the Ru(oxo) species is a more electrophilic oxidant than *t*-BuOOH, it is also most likely that the Ru(oxo) species is involved in the oxidation of free phosphine. Once formed, the Ru(salen)-oxo complex **5a** or **5b** proceeds to catalyse the oxidation of hydroxamic acid **1** to the corresponding acyl nitroso **27**. This oxidation can occur in two ways: either as a concerted or stepwise process. In the concerted pathway, deprotonation of hydroxamic acid by Ru(oxo) **5a** occurs simultaneously with hydride transfer from the hydroxamic acid **1** to the metal centre resulting in an acyl nitroso species **27** and metal hydride complex **28**. The Ru(salen) hydride complex **28** quickly loses water and is subsequently reoxidised to Ru(oxo)(salen) **5a** by *t*-BuOOH. Alternatively, the oxidation could proceed in a stepwise manner very similar to the well documented reactions between hydroxylamines and metals.^[18] Following initial deprotonation by the metal-oxo species, hydroxamic acid **1** can coordinate to the metal centre through the terminal oxygen, with the resulting intermediate **29** then collapsing to expel the acyl nitroso **27** and water from the coordination sphere of the catalyst. After the collapse, the complex is oxidised back to the Ru(oxo) **5a** and returns to the beginning of the catalytic cycle. Although both pathways are possible, we believe that stepwise process is more likely, since it is analogous to the well established oxidation of alcohols with PCC/TPAP^[19] and does not require a hydride transfer. Whichever route the oxidation takes, it results in a free, very reactive, acyl nitroso species which rapidly reacts with dienes *via* a conventional cycloaddition process to give adducts such as **3**. Since this seems to occur outside the coordination sphere of the catalyst, the reaction generally proceeds without selective asymmetric induction, at least in the intermolecular cycloaddition process.

The fact that there is no acceleration of the reaction or asymmetric induction in the product **11** during the cycloadditions using nitrosotoluene **10** [Eq. (4)], further confirms our hypothesis that acyl nitroso is not bound to the catalyst during the DA step. Furthermore, Ru(III)-(BINAP) complex **20** was found to be inactive as a catalyst in nitrosopyridine cycloadditions indicating that ruthenium metal is a poor catalyst for such Diels–Alder processes. Again, this confirms that the catalysts used so far in the oxidation of hydroxamic acids are excellent for the oxidation step, however they are not involved in the subsequent hetero-Diels–Alder step.



Scheme 3. Proposed mechanism for oxidation of hydroxamic acids with *in situ* Diels–Alder trapping of the acyl nitroso derivative as catalysed by Ru(salen)(PPh₃)₂ **4**.

Conclusions

We have postulated on the mechanism of the oxidation of hydroxamic acids and explained why the subsequent cycloaddition occurs without asymmetric induction in the product. In previous work, we and others have shown that complexes **4**, **12–16** are good catalysts for the oxidation step,^[7,8] in view of the results obtained from the screening of nitrosopyridine we need to review catalytic systems in order to carry out the oxidation and cycloaddition on the same metal centre. We know that Cu(II)-(BINAP) can catalyse a cycloaddition reaction between nitrosopyridine **21** and diene **2** with good levels of enantioselectivity, and that a combination of Cu(II) and pyridine moiety is essential at this point, however we need to understand the intrinsic nature of the Cu/nitrosopyri-

dine interactions if we are to design a catalyst with is capable of catalysing both the oxidation and Diels–Alder reactions. The work to develop such asymmetric catalysts is currently being undertaken in our laboratory and the results will be presented in the due course.

Experimental Section

General Methods

Where applicable, glassware was oven dried (130 °C) before use and cooled under a positive pressure of argon. All dry solvents were dried using a commercial drying system. All other materials were purchased directly from standard chemical suppliers and used without further purification unless otherwise stated. TLC was performed on plastic-

backed silica gel plates PET backed plates with visualisation achieved using a UV lamp or staining with K_2MnO_4 solution. Drying was carried out over anhydrous $MgSO_4$, followed by filtration. Evaporations were carried out at 20 mmHg using a rotary evaporator and water bath, followed by evaporation to dryness under vacuum (<2 mmHg). Purification by medium pressure column chromatography was performed using silica gel 35–70 μm . Melting points are uncorrected. All 1H and ^{13}C NMR were recorded on either 400 MHz or 500 MHz Bruker spectrometers. Chemical shifts are expressed as parts per million (ppm) downfield from the internal standard TMS. Asymmetric induction was determined using an HPLC system and UV/vis detector. Time-resolved IR was recorded on ReactIR 4000 and data manipulated using Mettler-Toledo ReactIR 3.0 software. CV was recorded on Autolab PGSTAT-30 in DCM using $n-Bu_4NF$ as electrolyte and Cp^* as internal reference.

Synthesis of Nitrosopyridine 21

A solution of *N*-chlorosuccimide (1.36 g, 10.2 mmol) in DCM (40 mL) was added dropwise to solution of 6-amino-2-picoline (1.00 g, 9.20 mmol) and dimethyl sulfide (0.75 mL, 10.2 mmol) in DCM (15 mL) at $-10^\circ C$ over a 1.5 hour period. The reaction mixture was stirred for one hour at $-10^\circ C$ and then for an additional hour at room temperature. Sodium methoxide (25 w/v% in MeOH, 4 mL, 18 mmol) was then added and resultant suspension was stirred for 10 min after which water (15 mL) was added and final mixture was stirred for an additional 1.5 h. The organic layer was separated and the aqueous layer was extracted with DCM (50 mL). The combined organic phases were washed with brine (100 mL), dried over $MgSO_4$ and filtered. The filtrate was concentrated under reduced pressure to give yellow residue (1H NMR spectroscopy indicated 1:7.5 ratio of starting material to product). This residue was then redissolved in DCM (10 mL) and added in one portion to an ice-cold solution of *m*CPBA (77% max, 2.33 g, 10 mmol) in DCM (40 mL). The reaction mixture was stirred for 10 min until a green colour became dominant and then dimethyl sulfide (0.34 mL, 4.61 mmol) was injected into the solution and the reaction mixture was stirred for a further 5 min. The green solution was then poured into saturated solution of Na_2CO_3 (30 mL) and the layers were separated. The aqueous phase was washed with additional portion of DCM (25 mL). The organic phases were combined, dried over $MgSO_4$ and filtered. The solvent was removed under reduced pressure on the rotary evaporator (water bath of which was kept at $5^\circ C$) to give a brown solid. The product was purified by silica gel chromatography (ethyl acetate: hexane, 1:2 as eluent). The blue-green fractions were combined and upon solvent removal the colour turned brown-yellow. The solid (yield: 0.39 g, 35%) could be stored in a fridge at $4^\circ C$ for up to 2 months. All spectroscopic and analytical data was identical to those reported.^[13]

Synthesis of *N,N'*-Bis(6-methyl-pyridin-2-yl)-diazene *N*-Oxide 26

A solution of *N*-chlorosuccimide (1.48 g, 11.1 mmol) in DCM (50 mL) was added dropwise to an ice-cold solution of 6-amino-2-picoline (1.00 g, 9.20 mmol) and dimethyl sulfide (0.82 mL, 11.1 mmol) in DCM (15 mL). The reaction

mixture was stirred for one hour at $0^\circ C$ and then for an additional hour at room temperature. Sodium methoxide (25 w/v% in MeOH, 4 mL, 18 mmol) was then added and resultant suspension was stirred for 10 min after which water (15 mL) was added and final mixture was stirred for an additional hour. The organic layer was separated and the aqueous layer was extracted with DCM (50 mL). The combined organic phases were washed with brine (100 mL), dried over $MgSO_4$ and filtered. The filtrate was concentrated under reduced pressure to give a yellow residue which was used in the next step without purification. 1H NMR spectroscopy indicated a 1:4 ratio (starting material:product).

A solution of sulfilimine from the first step (1.0 g, 5.9 mmol) in DCM (10 mL) was slowly added to an ice-cold solution of *m*CPBA (77% max, 1.76 g, 7.13 mmol) in DCM (30 mL). Upon addition the reaction mixture turned green. The reaction mixture was then stirred for 1 hour at $0^\circ C$ during which it became brown-red. Dimethyl sulfide (0.22 mL, 2.95 mmol) was added to the solution and the reaction was then stirred for an additional hour at room temperature. A saturated solution of Na_2CO_3 (30 mL) was added in and the layers were separated. The organic phase was washed with water (2×30 mL), dried over $MgSO_4$ and filtered. The solvent was removed under reduced pressure to give a brown solid. The product was obtained from diethyl ether as a brown-red crystalline solid (0.45, 66%) g, and the structure was confirmed by single crystal X-ray crystallography; mp $85-87^\circ C$. 1H NMR: (400 MHz, $CDCl_3$): $\delta = 2.59$ (s, 3H), 2.65 (s, 3H), 7.12 (d, $J = 7.6$ Hz, 1H), 7.37 (d, $J = 7.6$ Hz, 1H), 7.12 (t, $J = 7.8$ Hz, 1H), 7.80 (t, $J = 8.0$ Hz, 1H), 8.12 (d, $J = 8.0$ Hz, 1H), 8.17 (d, $J = 7.8$ Hz, 1H); ^{13}C NMR (400 MHz, $CDCl_3$): $\delta = 24.2, 24.4, 224.7, 115.4, 123.5, 126.8, 138.0, 139.1, 155.7, 157.0, 158.6, 158.7$; IR (NaCl film): $\nu_{max} = 3058$ (w), 1606 (m), 1591 (m), 1560 (m), 1477 (s), 1449 (s), 1375 (m), 1340 (m), 1272 (m), 1207 (m), 1167 (m), 1095 (w), 1082 (w), 1037 (w), 998 (m), 922 (w), 853 (m), 815 (m), 796 (m), 728 (m), 699 (w), 670 (w), 624 (w), 600 (w), 552 cm^{-1} (w); HR-MS (ES): $m/z = 229.1086$ [$M + H$]⁺ ($C_{12}H_{12}N_4O$ requires 229.1084); anal. found (%): C 62.67, H 5.34, N 23.60 ($C_{12}H_{12}N_4O$ requires C 63.15, H 5.30, N 24.55) (N.B. 1H NMR shows DMSO solvent impurity at 1/50 level).

Preparation of μ -Alkoxo-(1-[(2-hydroxy-3,5-di-*tert*-butylbenzylidene)-amino]-indan-2-ol)copper(II) Complex 16

$Cu(MeCN)_4ClO_4$ (89 mg, 0.27 mmol) was added in one portion to a stirred solution of (1*S*,2*R*)-1-[(2-hydroxy-3,5-di-*tert*-butylbenzylidene)amino]indan-2-ol (100 mg, 0.27 mmol) in DCM (5 mL). The reaction mixture was stirred for 1 hour after which it was washed with brine (10 mL). The green organic phase was collected, dried ($MgSO_4$), filtered, and concentrated under reduced pressure to give product **11** as a blue-green solid; yield: 74 mg (63%); mp $98-100^\circ C$. Anal. found (%): C 66.49, H 7.48, N 2.49 ($C_{48}H_{58}Cu_2N_2O_4 \cdot \text{hexane} \cdot 0.5\text{DCM}$ requires C 66.61, H 7.49, N 2.85); IR: $\nu_{max} = 2958$ (s), 1647 (vs), 1623 (vs), 1528 (m), 1459 (m), 1432 (m), 1385 (m), 1362 (m), 1322 (m), 1271 (m), 1255 (m), 1168 (m); 1053 (m), 749 (m), 535 cm^{-1} (m); HR-

MS (ES): $m/z = 853.3055$ $[M+H]^+$ [$C_{48}H_{58}Cu_2N_2O_4$ requires 853.3061 (^{63}Cu)].

Typical Procedure: NMR-Based Oxidation of Hydroxamic Acid **1** and Nitroso-Diels–Alder Reaction

Hydroxamic acid **1** (15 mg, 0.088 mmol) and catalyst **4** (0.7 mg, 0.88×10^{-3} mmol) were dissolved in DCM- d_2 (0.75 mL). Diene **2** (17 μ L, 0.19 mmol) and anisole (9.8 μ L, 0.088 mmol) were added into the mixture. At this point a 1H NMR spectrum was taken thus allowing for better shimming. A solution of *t*-BuOOH in hexane (5.5 M, 23 μ L, 0.13 mmol) was added instantly and the progress of the reaction was monitored by 1H NMR spectroscopy. The same procedure was used to follow the reactions with other dienes and the intramolecular case. The product can be isolated a following previously reported procedure.^[5b] The enantiomers could be separated by chiral HPLC (Chiracel OD, 10% EtOH in hexane, flow 1 mL min $^{-1}$, R_{t1} = 11 min, R_{t2} = 13 min or 10% IPA in hexane, flow 1 mL min $^{-1}$, R_{t1} = 19 min, R_{t2} = 21 min).

Typical Procedure: NMR-Based Diels–Alder Reaction of Nitrosotoluene

Nitrosotoluene **10** (15 mg, 0.12 mmol) and anisole (13.5 μ L, 0.12 mmol) were dissolved in DCM- d_2 (0.75 μ L). At this point a 1H NMR spectrum was taken thus allowing for better shimming. Diene (12 μ L, 0.12 mmol) was added instantly and the progress of the reaction was monitored by 1H NMR spectroscopy. The same procedure was used to follow the reactions with ruthenium complexes in it. Enantiomers could be separated by chiral HPLC (Chiracel OK, 10% IPA in hexane, flow 1 mL min $^{-1}$, R_{t1} = 18 min, R_{t2} = 24 min or Chiracel OJ, 10% IPA in hexane, flow 1 mL min $^{-1}$, R_{t1} = 19 min, R_{t2} = 29 min).

Typical Procedure for the Cycloaddition of Nitrosopyridine **21** to Cyclohexadiene **2**

A Schlenk tube was charged with Cu(II)(OTf) $_2$ (4.4 mg, 0.012 mmol) and *R,R*-BINAP (11.1 mg, 0.012 mmol). DCM (2 mL) was added to the reaction vessel and the mixture was stirred at room temperature until all solid dissolved. (In cases where catalysts were pre-made, they were just dissolved in DCM). The reaction mixture was then cooled to $-70^\circ C$ using a cryostat and a solution of nitrosopyridine **1** (15 mg, 0.12 mmol) in DCM (0.5 mL) was added dropwise to the reaction mixture. Upon addition the colour of the reaction changed to dark blue then to brown (also depends on the metal centre). The reaction mixture was stirred for additional 10 min and then solution of cyclohexadiene (0.012 mL, 0.12 mmol) in DCM (0.5 mL) was added dropwise over a period of 1 hour. The reaction was maintained between -70 and $-55^\circ C$ for the period of 24 h during which samples were collected, filtered through a pad of silica and analysed by HPLC (Chiracel OJ, 10% IPA in hexane, flow 1 mL min $^{-1}$, R_{t1} = 27 min, R_{t2} = 39 min). In cases where product was purified by silica gel chromatography (hexane:ethyl acetate, 3:1 as eluent; R_f = 0.7) the spectroscopic data matched those previously reported.^[13]

Reaction between PPh $_3$ and Nitrosotoluene **10**

Triphenylphosphine (43 mg, 0.16 mmol, 1.0 equiv.) was added to a solution of 2-nitrosotoluene (20 mg, 0.16 mmol, 1.0 equiv.) in DCM- d_2 (0.75 mL) in an NMR tube at room temperature. The reaction was analysed by ^{31}P NMR. After 5 min, the peak corresponding to free phosphine disappeared and peak corresponding to phosphine oxide appeared. The reaction mixture was filtered through a pad of silica and solvent was removed under vacuum to give triphenylphosphine oxide (43 mg, 93%) as an off-white solid. 2-Methylanisole was also detected by 1H NMR spectroscopy, however it was not isolated.

Typical Procedure for the Oxidation of Sulfilimine **24** and *in situ* Nitroso-Diels–Alder

A solution of catalyst **15** (5.4 mg, 1 mol%), cyclohexadiene (62 μ L, 0.65 mmol, 1.1 equiv.) and sulfilimine **24** (100 mg, 0.59 mmol, 1.0 equiv.) in acetone (2 mL) at room temperature was treated with an aqueous solution of 33% w/v H $_2$ O $_2$ (72 μ L, 0.71 mmol, 1.2 equiv.). The reaction mixture was stirred for 16 h and then was diluted with DCM (10 mL). The organic phase was washed with brine, dried over MgSO $_4$ and concentrated under vacuum. The residue was purified by silica gel chromatography (petroleum ether:ethyl acetate, 4:1 as eluent) and product isolated as a white solid (yield: 49 mg, 42%) with analytical data matching that previously reported.^[13]

X-Ray Crystallography

An orange single crystal of **26** (0.15 \times 0.15 \times 0.20 mm) was analysed at 100(2) K on a Nonius Kappa CCD diffractometer using graphite monochromated Mo-K α radiation (λ = 0.71073 Å). Structure solution was carried out using SHELXS-97^[21] and refined by full matrix least squares in SHELXL-97.^[22] All non-hydrogen atoms were refined with anisotropic displacement parameters. Hydrogen atoms were positioned geometrically with isotropic displacement parameters fixed to ride on the parent atom [aromatic C–H 0.94 Å, U_{iso} = $1.2 \times U_{eq}(C)$; methyl C–H 0.98 Å, U_{iso} = $1.5 \times U_{eq}(C)$]. The asymmetric unit consisted of one molecule. The oxygen atom, O1, is modelled over two sites (N2 or N3) with a ratio of 35:65; the NMR data supports this assertion, indicating that there is only one oxygen atom per molecule. Selected bond lengths and angles are listed in Table 3. Crystal data for **26**: $M = 228.26$, monoclinic space group $P2_1$, $a = 6.2863(1)$, $b = 12.3951(3)$, $c = 7.8106(2)$ Å, $\beta = 112.623(1)^\circ$, $V = 561.77(2)$ Å 3 , $Z = 2$, $\rho_{calcd} = 1.349$ Mg/m 3 , $\mu = 0.0091$ mm $^{-1}$, $F(000) = 240$, 19627 reflections collected ($2.83 \leq \theta \leq 30.51^\circ$), 1778 independent reflections ($R_{int} = 0.0510$) were used for structure refinement, final $R_f = 0.0412$.

Table 3. Selected bond angles and lengths for structure **26**.

Bond Length [Å]		Angle [°]	
C(1)–N(2)	1.459(3)	C(1)–N(2)–N(3)	115.3(2)
C(7)–N(3)	1.453(3)	C(7)–N(3)–N(2)	115.1(2)
N(2)–N(3)	1.280(2)	N(2)–N(3)–O(1 A)	129.7(2)
N(3)–O(1 A)	1.329(3)		

$[F^2 > 2\sigma(F)]$, $wR_2 = 0.1043$ [$F^2 > 2\sigma(F)$], $R_1 = 0.0492$ (all data), $wR_2 = 0.1088$ (all data), GOF (F^2) = 1.036, largest peak, hole = 0.310, $-0.203 \text{ e \AA}^{-3}$. PLATON^[23] suggested the possible presence of a *c*-glide, however upon examining the reflection file significant intensities were found for the h0L reflections with (h+L) odd, which would be absent if the *c*-glide were real. CCDC reference number CCDC 663249.

Acknowledgements

We thank Professor Ken Shea (University of California, Irvine) for providing compound **8** and for helpful discussions, Dr Paul Low (Durham University) for assistance with cyclic voltammetry, and the EPSRC, Swansea Mass Spectrometry service.

References

- [1] G. W. Kirby, *Chem. Soc. Rev.* **1977**, 6, 1–24.
- [2] a) O. Wichterle, *Collect. Czech. Chem. Commun.* **1947**, ##43##12, 292; b) Y. A. Arbuzov, *Dokl. Akad. Nauk SSSR* **1948**, 60, 993–996; c) J. Hammer, A. Ahmad, R. E. Holliday, *J. Org. Chem.* **1963**, 28, 3034–3036; d) G. Kresze, J. Firl, H. Zimmer, U. Wollnik, *Tetrahedron* **1964**, 20, 1605–1611.
- [3] a) H. Yamamoto, N. Momiyama, *Chem. Commun.* **2005**, 3514–3525; b) Y. Yamamoto, H. Yamamoto, *Eur. J. Org. Chem.* **2006**, 2031–2043.
- [4] a) L. H. Dao, J. M. Dusk, D. Mackay, K. N. Watson, *Can. J. Chem.* 1979, **57**, 1712–1719; b) N. E. Jenkins, R. W. Ware, Jr., R. N. Atkinson, S. B. King, *Synth. Commun.* **2000**, **30**, 947–953.
- [5] a) K. R. Flower, A. P. Lightfoot, H. Wan, A. Whiting, *Chem. Commun.* **2001**, 1812–1813; b) A. P. Lightfoot, R. G. Pritchard, H. Wan, J. E. Warren, A. Whiting, *Chem. Commun.* **2002**, 2072–2073; c) J. A. K. Howard, G. Ilyashenko, H. A. Sparkes, A. Whiting, *Dalton Trans.* **2007**, 2108–2111.
- [6] S. Iwasa, K. Tajima, S. Tsushima, H. Nishiyama, *Tetrahedron Lett.* **2001**, 42, 5897–5899.
- [7] K. R. Flower, A. P. Lightfoot, H. Wan, A. Whiting, *J. Chem. Soc. Perkin Trans. 1* **2002**, 2058–2064.
- [8] C. P. Chow, K. J. Shea, *J. Am. Chem. Soc.* **2005**, **127**, 3678–3679.
- [9] a) M. E. Marmion, K. J. Takeuchi, *J. Am. Chem. Soc.* **1988**, **110**, 1472–1480; b) C. Che, W. Tang, W. Wong, T. Lai, *J. Am. Chem. Soc.* **1989**, **111**, 9048–9056.
- [10] a) T. S. Siddall, N. Miyaura, J. C. Huffman, J. Kochi, *J. Chem. Soc. Chem. Commun.* **1983**, 1185–1186; b) E. G. Samsel, K. Srinivasan, J. K. Kochi, *J. Am. Chem. Soc.* **1985**, **107**, 7606–7617.
- [11] BatchCAD v8, <http://www.aspentech.com/>.
- [12] S. E. Schaus, J. Brnalt, E. N. Jacobsen, *J. Org. Chem.* **1998**, **63**, 403–405.
- [13] Y. Yamamoto, H. Yamamoto, *J. Am. Chem. Soc.* **2004**, **126**, 4128–4129.
- [14] K. Mashima, T. Hino and H. Takaya, *J. Chem. Soc. Dalton Trans.* **1992**, 2099–2107.
- [15] S. Juge, J. P. Genet, S. Mallari, *PCT Int. Appl. WO* 9102588A1 19910307, **1991**.
- [16] a) E. C. Taylor, C. Tseng, J. B. Rampal, *J. Org. Chem.* **1982**, **47**, 552–555; b) S. Huang, D. Swern, *J. Org. Chem.* **1979**, **44**, 2510–2513.
- [17] J. Lee, L. Chen, A. H. West, G. B. Richter-Addo, *Chem. Rev.* **2002**, **102**, 1019–1065.
- [18] a) D. B. Sams, R. J. Doedens, *Inorg. Chem.* **1979**, **18**, 153–156; b) S. Clamp, N. G. Connelly, J. A. K. Howard, I. Manners, J. D. Payne and W. E. Geiger, *J. Chem. Soc. Dalton Trans.* **1984**, 1659–1665.
- [19] a) W. P. Griffith, S. V. Ley, G. P. Whitcombe, A. D. White, *J. Chem. Soc. Chem. Commun.* **1987**, 1625–1627; b) I. E. Markó, P. R. Giles, M. Tsukazaki, I. Chellé-Regnaut, C. J. Urch, S. M. Brown, *J. Am. Chem. Soc.* **1997**, **119**, 12661–12662.
- [20] a) N. Momiyama, H. Yamamoto, *Org. Lett.* **2002**, **4**, 3579; b) Y. Hayashi, J. Yamaguchi, T. Sumiya, K. Hibino, M. Shoji, *J. Org. Chem.* **2004**, **69**, 5966–5973; c) G. Zhong, *Chem. Commun.* **2004**, 606–607; d) G. Zhong, *Angew. Chem.* **2003**, **115**, 4379–4382; *Angew. Chem. Int. Ed.* **2003**, **42**, 4247–4250; e) Y. Yamamoto, N. Momiyama, H. Yamamoto, *J. Am. Chem. Soc.* **2004**, **126**, 5962–5963; f) N. Momiyama, H. Yamamoto, *J. Am. Chem. Soc.* **2003**, **125**, 6038–6039.
- [21] G. M. Sheldrick, *Acta Crystallogr. Sect. A* **1990**, **46**, 467–473.
- [22] G. M. Sheldrick, *Computer Program for Crystal Structure Refinement*, University of Göttingen.
- [23] A. L. Speck *PLATON, A Multipurpose Crystallographic Tool*, Utrecht University, Utrecht, The Netherlands, **1998**.